2017

# Single Nanotube Spectral Imaging To Determine Molar Concentrations of Isolated Carbon Nanotube Species

Thomas V. Galassi

Prakrit V. Jena

***See next page for additional authors***



Citation/Publisher Attribution

Galassi, T. V., Jena, P. V., Roxbury, D., & Heller, D. A. (2017). Single Nanotube Spectral Imaging To Determine Molar Concentrations of Isolated Carbon Nanotube Species. *Anal. Chem.*, *89*(2), 1073-1077. doi: 10.1021/acs.analchem.6b04091
Available at: https://doi.org/10.1021/acs.analchem.6b04091

HHS Public Access

Author manuscript

*Anal Chem*. Author manuscript; available in PMC 2017 July 17.

Published in final edited form as:

*Anal Chem*. 2017 January 17; 89(2): 1073–1077. doi:10.1021/acs.analchem.6b04091.

# Single nanotube spectral imaging to determine molar concentrations of isolated carbon nanotube species

**Thomas V. Galassi**[†,‡], **Prakrit V. Jena**[†], **Daniel Roxbury**[¥], and **Daniel A. Heller**[*,†,‡]

[†]Memorial Sloan Kettering Cancer Center, New York, NY 10065, United States

[‡]Weill Cornell Medical College, New York, NY 10065, United States

[¥]University of Rhode Island, Kingston, RI 02881, United States

## Abstract

Electronic and biological applications of carbon nanotubes can be highly dependent on the species (chirality) of nanotube, purity, and concentration. Existing bulk methods, such as absorbance spectroscopy can quantify SP2 carbon based on spectral bands, but nanotube length distribution, defects, and carbonaceous impurities can complicate quantification of individual particles. We present a general method to relate the optical density of a photoluminescent nanotube sample to the number of individual nanotubes. By acquiring 3-dimensional images of nanotubes embedded in a gel matrix with a reducing environment, we quantified the individual nanotubes in a volume, resulting in a measurement of all emissive nanotubes. Via spectral imaging, we assessed structural impurities and precisely determined molar concentrations of the (8,6) and (9,4) nanotube species. We developed an approach to obtain the molarity of any structurally-enriched semiconducting single-walled carbon nanotube preparation on a per-nanotube basis.

## Graphical Abstract

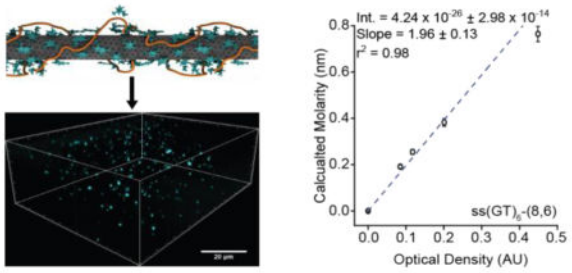


Semiconducting single-walled carbon nanotubes (SWCNTs) are a cylindrical form of nanocarbon that exhibit novel optical and electronic properties[1]. An as-produced nanotube

*Corresponding Author: hellerd@mskcc.org.

**Author Contributions**

The manuscript was conceived and written through contributions of all authors. T.V.G and P.V.J designed and performed the experiments, and analyzed data. All authors have given approval to the final version of the manuscript.

Supporting Information

The Supporting Information is available free of charge on the ACS Publications website and contains detailed materials and methods, and supplementary figures S1–12. (PDF)

sample is intrinsically heterogeneous, containing nanotubes with different diameters, lengths, and chiral angles. Nanotube optical and electronic properties are highly dependent on diameter and roll up angle, which are defined by two integers (n,m) denoting nanotube species/chirality[2]. Absorption spectroscopy is the most commonly used analytical technique for characterizing a solution dispersion of a carbon nanotube sample[2–4]. Using experimentally calculated molar extinction coefficients, the concentration of nanotubes in solution can be obtained in terms of mass per volume[5].

The characterization of SWCNT samples is confounded by their intrinsic heterogeneity. Although absorption cross sections are largely independent of average nanotube length[6], recent ensemble[7] and single-molecule studies[8] have revealed the chirality-dependent absorption cross section of SWCNTs. Moreover, the distribution of chiralities in a bulk nanotube sample can vary based on the sample preparation technique. As a result, the concentration of carbon nanotubes calculated from ensemble measurements[9] rely on extinction coefficients that may only be accurate for a specific sample preparation.

Current methods for mapping the chirality distribution of semiconducting carbon nanotubes include imaging approaches such as graphite-assisted atomic force microscopy (AFM), scanning tunneling microscopy (STM), transmission electron microscopy (TEM), electron diffraction, or spectroscopic techniques including Raman and photoluminescence spectroscopy[10]. Although photoluminescence excitation/emission (PLE) maps have emerged as the standard for analyzing semiconducting nanotubes in solution, artifacts such as bundling[11] and exciton energy transfer[12] can affect the PLE data.

The need for single-chirality semiconducting nanotubes for both electronic[13] and biomedical[1] applications has led to increasingly successful separation techniques. Variants of poly(9,9-di-n-octylfluorenyl-2,7-dyl) (PFO) have been used to selectively disperse and enrich specific SWCNT chiralities[14]. Surfactant-encapsulated SWCNTs have been sorted using density gradient ultracentrifugation[15], gel-chromatography[16], and polymer aqueous two-phase systems[17,18] to provide highly-purified single nanotube chiralities in large-scale yields. Separation of biocompatible ssDNA-nanotube complexes has been accomplished using ion-exchange (IEX) high performance liquid chromatography (HPLC)[19] and polymer aqueous two-phase systems[20]. The growth of single-chirality carbon nanotubes has also been demonstrated[21].

Despite advances in nanotube purification procedures and new applications of chirality-enriched nanotube samples, especially in biology and medicine[15,22–24], current techniques for determining absorption coefficients for chirality-enriched SWCNT samples are lacking. Existing, indirect methods for calculating absorption coefficients require assumptions and introduce systematic uncertainties; reported absorption coefficients for the (6,5) nanotube vary over orders of magnitude[7,25–27]. Recently, absolute absorption cross sections of several SWCNT chiralities dispersed with sodium cholate or poly(9,9-di-n-octylfluorenyl-2,7-dyl) (PFO) were directly determined and normalized per carbon atom[28]. This was accomplished using 2D-short wave infrared (SWIR) fluorescence imaging to directly count individual SWCNTs within a precisely-constructed microfluidic chamber filled with sorbitol.

Techniques to directly determine SWCNT absorption cross sections have been limited to bright surfactant and polymer-encapsulated SWCNTs. Thus, despite the high purity separation afforded by ssDNA-nanotubes, techniques to characterize the sample concentration are limited by the lower quantum yield of ssDNA nanotube preparations. Moreover, the aforementioned absorption coefficients, reported in units of $cm^2$ per carbon atom and mass per volume, are not optimal for certain applications, such as biological sensing in live cells, wherein each fluorescent nanotube represents a distinct sensing element[24]. Knowledge of the nanotube concentration in terms of sensing elements per unit volume will allow improved control over the sensor/analyte ratio. Additionally, in the fabrication of electronics, the transfer characteristics, threshold voltage, and even field effect mobility can depend on the nanotube deposition density on the device[29]. Thus, a technique for obtaining nanotube concentration and chirality information at the single-nanotube level would be valuable for multiple fields.

Here, we report a single nanotube counting method to relate the molar concentration of chirality-enriched semi-conducting SWCNTs to the optical density (OD) measured in solution. Using a near-infrared microscopy system coupled to a piezo z-axis stage, we explicitly counted emissive nanotubes within an optically-defined volume. The bright emission intensity of IEX-purified (8,6) and (9,4) nanotube chiralities embedded in an agarose gel, acquired following on-resonance excitation with a 730 nm laser, was further enhanced using a reducing agent[30]. We used hyperspectral microscopy to assess the monodispersity of nanotube chiralities on the single-nanotube level and correct for impurities[31]. The number of imaged nanotubes scaled linearly with the absorbance peak of the first electronic transition ($E_{11}$) thereby directly relating the experimentally determined molar concentrations of chirality-separated (8,6) and (9,4) nanotube samples with their absorption bands. The generalizability and accuracy of this method in determining molarity could enable investigators to obtain chirality-specific concentrations of any semiconducting carbon nanotube preparation.

## EXPERIMENTAL SECTION

Detailed information on the chemical reagents used, preparation of the ssDNA-nanotube dispersions, IEX purification, instrumentation, data acquisition, and analysis are provided in the Supporting Information.

### Preparation of chirality-enriched DNA-SWCNT samples

Single-walled carbon nanotubes produced by the HiPco process (Unidym) were suspended via sonication with single-stranded DNA for 30 minutes, followed by 30 minutes of ultracentrifugation. The $(CCG)_4$ and $(GT)_6$ ssD-NA oligonucleotides were used to selectively enrich the (9,4) and (8,6) species, respectively, using IEX-HPLC[19]. The purity of each sample was assessed both via absorption spectroscopy (Figure 1) and two-dimensional photoluminescence excitation/emission spectroscopy (Figure S1), while length distributions were assessed with atomic force microscopy (Figure S2).

### Hyperspectral microscopy

Hyperspectral microscopy, a recently developed technique that allows every pixel of a near-infrared fluorescent image to be spectrally resolved[31], was used both to correct for impurities in chirality-enriched SWCNT samples, as well as to confirm that single regions of interest (ROI's) within agarose gels did not represent nanotube bundles or aggregates.

### Immobilization and direct counting of ssDNA-SWCNTs

To directly count the number of fluorescent DNA-SWCNTs within known volumes, the nanotubes were immobilized at four different dilution factors in 1% low melt agarose gels. The intensity of nanotube emission within the gels was increased via supplementation with reducing agents which are known to enhance the photoluminescence quantum yield of carbon nanotubes (Figure 2, S3)[30].

Nanotubes were excited at 730 nm, nearly on-resonance with both the (8,6) and (9,4) species, and imaged using a 2D near-infrared InGaAs detector. We used a 100X (1.40 NA) oil objective to excite a ~ 90 μm diameter area with a 2W CW laser. Due to power loss through beam shaping optics, this resulted in a power density of ~ 10.0 kW/cm$^2$ at the sample. Using an automated stage with z-axis control, 3 dimensional image stacks were acquired with a 200 nm step size to optically define the imaging volume. This allowed for nanotubes to be imaged and directly counted for each dilution of the chirality-enriched samples within volumes of 154 pL, using ImageJ. For each nanotube chirality, the number of emissive nanotubes was counted in 3 sections per agarose gel and for 3 gels per dilution factor for a total of nine technical replicates per sample/dilution factor.

## RESULTS AND DISCUSSION

Prior to performing nanotube counting experiments, we tested the effect of reducing agents on nanotube emission from within 1% agarose gels. In solution, the presence of reducing agents is known to increase the fluorescence intensity of DNA-SWCNTs[30]. This occurs due to the passiviation of defective SWCNTs via the donation of electrons to SWCNT sidewalls[30]. A similar effect was seen in agarose gels, as supplementing gels with reducing agents such as ascorbic acid or Trolox resulted in an increase in the intensity of DNA-SWCNTs embedded in gels and was stable for over 3 hours (Figure 2, S3–4). Thus, for all counting experiments, 1% agarose gels were supplemented with 2 mM Trolox (Figure 3).

Hyperspectral microscopy of Trolox-supplemented agarose gels containing unsorted ss(GT)$_6$-SWCNTs showed a single emission peak for over 97% of the ROI's, confirming that single nanotubes could be observed and that the DNA-nanotube complexes represented individual nanotubes instead of bundles or aggregates (Figure S5).

We counted individual nanotubes within the gels at four dilution factors of the stock sample concentration. To ensure that we were not systematically undercounting shorter and dimmer nanotubes, we adapted a technique from Streit et al[32]. Trolox-supplemented agarose gels containing the (GT)$_6$-(8,6) sample were imaged under different excitation powers. As the excitation power was increased from 1.12 kW/cm$^2$ to 9.12 kW/cm$^2$, the average number of nanotubes detected per field of view increased from 1.7 to 22.3 (Figure S6). However, when

the excitation power was increased further to 12.9 kW/cm$^2$, no statistically significant increase in the number of detected nanotubes was observed, and a logistic fit of the data suggested that no further increase would be seen with increasing laser power (Figure S6). Since all counting experiments were performed at 12.9 kW/cm$^2$, this suggests that we did not systematically undercount dim nanotubes. Inspection of SWCNT absorption spectra shows distinct nanotube peaks with relatively low background (Figure S7), indicating that the sample did not contain a large fraction of defective and thus dark SWCNTs[33,34]. When counting both the ss(CCG)$_4$-(9,4) and ss(GT)$_6$-(8,6) enriched samples, the number of nanotubes detected in the gels scaled linearly with dilution factor, with $r^2$ values of 0.97. This number increased to 0.99 for both samples after applying the mild assumption that a dilution factor of 0 yields a SWCNT count of 0 (Figure S8). The strong linear relation between the sample dilution and the number of individual nanotubes counted indicates the robustness and accuracy of the counting methodology.

To effectively determine the molarity of the (8,6) and (9,4) chiralities specifically, a correction factor was established to account for the other chiralities that may have been observed in the agarose gels. For the (8,6)-enriched sample, examination of its PL plot (Figure S1) indicates the presence of an impurity in the form of the (9,5) nanotube. Using hyperspectral microscopy, emission spectra were acquired for 384 nanotubes adsorbed to a glass surface under 730 nm excitation. Upon fitting the emission spectra of each nanotube to assign chirality, 381 nanotubes were identified as the (8,6) species (Figure S9), indicating that although (9,5) nanotubes were present in the sample, they were not easily visualized with off resonance excitation, and they did not significantly contribute to the nanotube counts. Thus, for the (8,6) chirality, only a small correction factor of 0.992 was required.

Examination of the PL plot of the (9,4) sample (Figure S1) showed a significant amount of impurities in the form of the (7,6) nanotube which emits in a similar range as the (9,4) chirality but has a different excitation maximum. Thus, we developed an alternate approach to correct for the impurities.

We first used hyperspectral microscopy to assess chiralities emitting at different wavelengths than the (9,4) species. Using hyperspectral microscopy, we found that 4% (10/236) of nanotubes observed in the sample emitted at wavelengths denoting chiralities other than (7,6) or (9,4). Due to their overlapping emission bands, the (7,6) and (9,4) nanotubes could not be spectrally resolved.

We then developed a method to assess other chiralities with the same emission wavelength but different excitation wavelengths. In brief, nanotubes from the (9,4) enriched sample were immobilized on a glass surface. Due to the differing excitation maxima of the (9,4) and (7,6) nanotubes, these chiralities were resolved by exciting the sample and acquiring images sequentially with 730 nm and 660 nm lasers set to the same power. Nanotubes emitting under 730 nm excitation were then analyzed under 660 nm excitation to determine the effect on emission intensity (Figure 4). A total of 240 nanotubes were analyzed, out of which 33 became brighter under 660 nm excitation. We thus obtained a correction factor of 0.86; i.e., 14% of the nanotubes detected under 730 nm excitation were actually the (7,6) species.

To determine a final correction factor for the (9,4) sample, the correction factor that was determined via hyper-spectral microscopy (0.96), was multiplied by the correction factor that was determined via the differing excitation maxima of the (9,4) and (7,6) nanotubes (0.86). This gave a final correction factor of 0.82. Corrected molarities of single nanotubes scaled linearly with the dilution factor of the sample from the initial stock (Figure 5). The $r^2$ values were greater than 0.99 for both samples after carrying over the assumption that a dilution factor of 0 corresponds to a nanotube count of 0. The line was then used to extrapolate the molarity of the nanotube samples at higher concentrations suitable for ensemble absorbance measurements. Baseline subtraction was performed on the absorbance spectra of each sample at these dilutions, such that the $E_{11}$ absorption peaks could be related to the molarity of each chirality-resolved nanotube species (Figure S10–11). For the $ss(CCG)_4$-(9,4) sample, this required deconvolution of the (9,4) and (7,6) absorption peaks (Figure S12).

From these calculations, we plotted the extrapolated nanotube molarities against OD of the corresponding sample dilution, once again applying the previously described assumption regarding an optical density of 0 AU. Linear fits of calculated molarity vs. OD for the (9,4) and (8,6) samples gave $r^2$ values of 0.99 and 0.98, respectively (Figure 5). This linear relationship is derived purely from experimental data for this particular sample and does not rely on references, calculations, or tabulated values from different sample preparations. Taking into account the 1 cm path length used for absorbance measurements, we can calculate molar absorptivity/extinction coefficients on a per nanotube basis for our samples. These calculations gave values of 0.205 $nM^{SWCNT-1} \cdot cm^{-1}$ and 0.510 $nM^{SWCNT-1} \cdot cm^{-1}$ for the (9,4) and (8,6) samples respectively.

The above values differ from previously reported extinction coeficcients and absorption cross sections in that they are normalized by nanotube concentration rather than the number of carbon atoms in the sample, making them more relevant to biosensing and imaging related applications. It is important to note however, that unlike previously reported absorption cross sections for the $E_{11}$ absorption peak ($\sigma_{11}$)[28,35,36], the values reported here are dependent on the SWCNT length distribution, as two SWNT preparations with varying length distributions may contain equal concentrations of carbon atoms despite containng different numbers of nanotubes per unit volume. This highlights the importance of applying the developed method to individual SWCNT preparations. To convert the values obtained using the described method to the carbon atom based $\sigma_{11}$ values reported elsewhere, one only needs to take into account the average nanotube length and the number of carbon atoms present per nm for the SWCNT chirality of interest. Converting the per nanotube extinction coefficients to absorption cross sections in units of $cm^2$/carbon atom ($C_{atom}$) gives values of $5.15 \times 10^{-17}$ $cm^2/C_{atom}$ and $18.56 \times 10^{-17}$ $cm^2/C_{atom}$, for the (9,4) and (8,6) samples respectivey, which fall well within the range of previously published values[28,35,36].

## Conclusion

In this work, we described the development of a set of imaging methods to relate DNA-nanotube OD at the $E_{11}$ to concentration, in terms of the emissive nanotube number per unit volume or molarity, for any structurally-enriched semiconducting SWCNT preparation. We

applied this method to map OD to molarity for the (8,6) and (9,4) nano-tubes and calculate their extinction coefficients based on the number of individual nanotubes rather than total graphitic carbon. This method is applicable to any chirality-enriched nanotube sample. The technique allows one to account for relatively dim nanotube preparations and use commercially available instrumentation. The straightforward data acquisition and analysis could facilitate the use of this method for routine sample characterization. Such methods are useful for many SWCNT-based applications, particularly electronic and biomedical applications where semiconducting nanotubes function as important components, and where interactions with living systems are important.

## Supplementary Material

Refer to Web version on PubMed Central for supplementary material.

## Acknowledgments

This work was supported in part by the NIH New Innovator Award (DP2-HD075698), the Cancer Center Support Grant (P30 CA008748), the Anna Fuller Fund, the Louis V. Gerstner Jr. Young Investigator's Fund, the Frank A. Howard Scholars Program, the Honorable Tina Brozman Foundation for Ovarian Cancer Research, Cycle for Survival, the Alan and Sandra Gerry Metastasis Research Initiative, Mr. William H. Goodwin and Mrs. Alice Goodwin and the Commonwealth Foundation for Cancer Research, the Experimental Therapeutics Center, the Imaging & Radiation Sciences Program, and the Center for Molecular Imaging and Nanotechnology of Memorial Sloan Kettering Cancer (MSKCC). P.V.J was supported by an NIH NCI T-32 fellowship (2T32CA062948-21). D.R. was supported by an American Cancer Society 2013 Roaring Fork Valley Research Fellowship. We thank the Molecular Cytology Core Facility at MSKCC for imaging software support. We would like to thank J. Streit for helpful discussions throughout the preparation of this manuscript.

## References

1. Hong G, Diao S, Antaris AL, Dai H. Chem Rev. 2015; 115:10816–10906. [PubMed: 25997028]
2. Bachilo SM, Strano MS, Kittrell C, Hauge RH, Smalley RE, Weisman RB. Science. 2002; 298:2361–2366. [PubMed: 12459549]
3. Naumov AV, Ghosh S, Tsyboulski DA, Bachilo SM, Weisman RB. ACS Nano. 2011; 5:1639–1648. [PubMed: 21341755]
4. Strano MS, Doorn SK, Haroz EH, Kittrell C, Hauge RH, Smalley RE. Nano Lett. 2003; 3:1091–1096.
5. Schoppler F, Mann C, Hain TC, Neubauer FM, Privitera G, Bonaccorso F, Chu DP, Ferrari AC, Hertel T. J Phys Chem C. 2011; 115:14682–14686.
6. Naumov AV, Tsyboulski DA, Bachilo SM, Weisman RB. Chemical Physics. 2013; 422:255–263.
7. Vialla F, Roquelet C, Langlois B, Delport G, Santos SM, Deleporte E, Roussignol P, Delalande C, Voisin C, Lauret JS. Phys Rev Lett. 2013; 111:137402. [PubMed: 24116816]
8. Liu KH, Hong XP, Choi S, Jin CH, Capaz RB, Kim J, Wang WL, Bai XD, Louie SG, Wang EG, Wang F. Proc Natl Acad Sci USA. 2014; 111:7564–7569. [PubMed: 24821815]
9. Nair N, Usrey ML, Kim WJ, Braatz RD, Strano MS. Anal Chem. 2006; 78:7689–7696. [PubMed: 17105160]
10. Zhao QC, Zhang J. Small. 2014; 10:4586–4605. [PubMed: 25330979]
11. Torrens ON, Milkie DE, Zheng M, Kikkawa JM. Nano Lett. 2006; 6:2864–2867. [PubMed: 17163720]
12. Lefebvre J, Finnie P. J Phys Chem C. 2009; 113:7536–7540.
13. Wang C, Takei K, Takahashi T, Javey A. Chem Soc Rev. 2013; 42:2592–2609. [PubMed: 23229523]
14. Nish A, Hwang JY, Doig J, Nicholas R. J Nat Nanotechnol. 2007; 2:640–646.

15. Ghosh S, Bachilo SM, Weisman RB. Nat Nanotechnol. 2010; 5:443–450. [PubMed: 20453856]
16. Liu HP, Nishide D, Tanaka T, Kataura H. Nat Commun. 2011; 2
17. Fagan JA, Khripin CY, Silvera Batista CA, Simpson JR, Hároz EH, Hight Walker AR, Zheng M. Adv Mat. 2014; 26:2800–2804.
18. Khripin CY, Fagan JA, Zheng MJ. Am Chem Soc. 2013; 135:6822–6825.
19. Tu X, Manohar S, Jagota A, Zheng M. Nature. 2009; 460:250–253. [PubMed: 19587767]
20. Ao G, Khripin CY, Zheng M. J Am Chem Soc. 2014; 136:10383–10392. [PubMed: 24976036]
21. Sanchez-Valencia JR, Dienel T, Groning O, Shorubalko I, Mueller A, Jansen M, Amsharov K, Ruffieux P, Fasel R. Nature. 2014; 512:61. [PubMed: 25100481]
22. Sun P, Bachilo SM, Weisman RB, Nagarajaiah S. J Strain Anal Eng Des. 2015; 50:0309324715597414.
23. Hong G, Diao S, Chang J, Antaris AL, Chen C, Zhang B, Zhao S, Atochin DN, Huang PL, Andreasson KI, Kuo CJ, Dai H. Nat Photon. 2014; 8:723–730.
24. Giraldo JP, Landry MP, Kwak SY, Jain RM, Wong MH, Iverson NM, Ben-Naim M, Strano MS. Small. 2015; 11:3973–3984. [PubMed: 25981520]
25. Harrah DM, Schneck JR, Green AA, Hersam MC, Ziegler LD, Swan AK. ACS Nano. 2011; 5:9898–9906. [PubMed: 22077149]
26. Berciaud S, Cognet L, Lounis B. Phys Rev Lett. 2008; 101:077402. [PubMed: 18764579]
27. Oudjedi L, Parra-Vasquez ANG, Godin AG, Cognet L, Lounis B. J Phys Chem Lett. 2013; 4:1460–1464. [PubMed: 26282299]
28. Streit JK, Bachilo SM, Ghosh S, Lin CW, Weisman RB. Nano Lett. 2014; 14:1530–1536. [PubMed: 24502235]
29. Takahashi T, Takei K, Gillies AG, Fearing RS, Javey A. Nano Lett. 2011; 11:5408–5413. [PubMed: 22050705]
30. Lee AJ, Wang X, Carlson LJ, Smyder JA, Loesch B, Tu X, Zheng M, Krauss TD. Nano Lett. 2011; 11:1636–1640. [PubMed: 21417364]
31. Roxbury D, Jena PV, Williams RM, Enyedi B, Niethammer P, Marcet S, Verhaegen M, Blais-Ouellette S, Heller DA. Sci Rep. 2015; 5:14167. [PubMed: 26387482]
32. Streit JK, Bachilo SM, Naumov AV, Khripin C, Zheng M, Weisman RB. ACS Nano. 2012; 6:8424–8431. [PubMed: 22924324]
33. Fagan JA, Hároz EH, Ihly R, Gui H, Blackburn JL, Simpson JR, Lam S, Hight Walker AR, Doorn SK, Zheng M. ACS Nano. 2015; 9:5377–5390. [PubMed: 25871430]
34. Khripin CY, Tu X, Heddleston JM, Silvera-Batista C, Hight Walker AR, Fagan J, Zheng M. Anal Chem. 2013; 85:1382–1388. [PubMed: 23259532]
35. Malapanis A, Perebeinos V, Sinha DP, Comfort E, Lee JU. Nano Lett. 2013; 13:3531–3538. [PubMed: 23899132]
36. Sanchez SR, Bachilo SM, Kadria-Vili Y, Lin CW, Weisman RB. Nano Lett. 2016

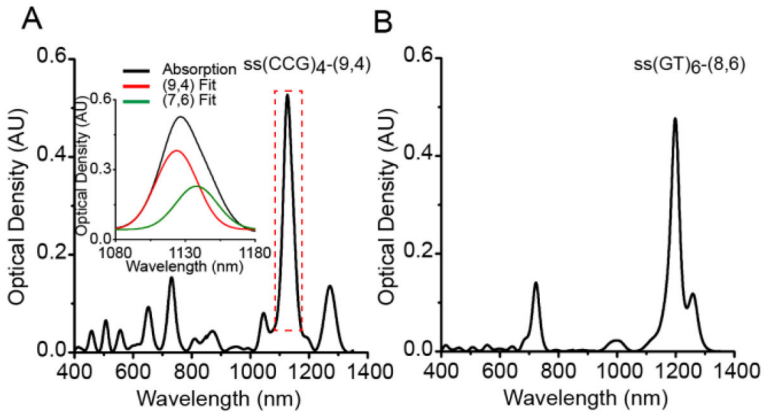


**Figure 1.**

Baseline-subtracted absorption spectra of chirality-enriched ssDNA-nanotube samples. A) Absorption spectrum of the (9,4)-enriched ss$(CCG)_4$-SWCNT sample. Inset: Deconvolution of the (9,4) electronic transition peak from the (7,6) electronic transition peak. B) Absorption spectrum of the (8,6)-enriched ss$(GT)_6$-SWCNT sample.

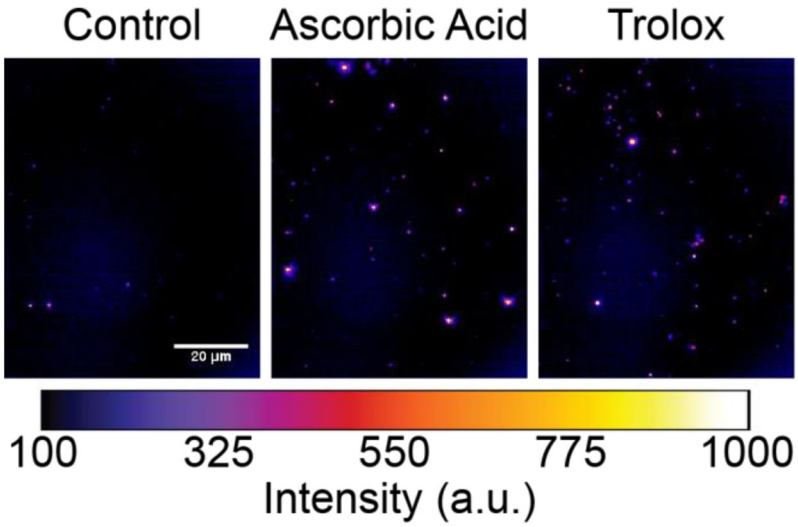


**Figure 2.**
Near infrared images of DNA-SWCNTs within agarose gels supplemented with ascorbic acid or Trolox.

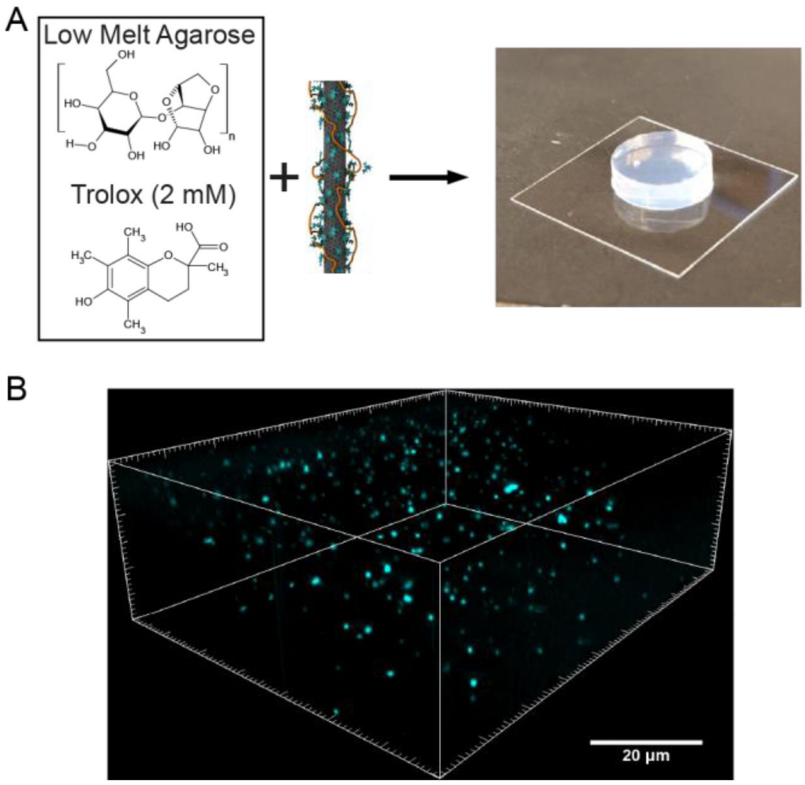


**Figure 3.**

Imaging single emissive SWCNTs immobilized in an agarose gel. A) Schematic of nanotube immobilization procedure. B) A deconvolved 3D image of the agarose gel showing emission of single nanotubes.

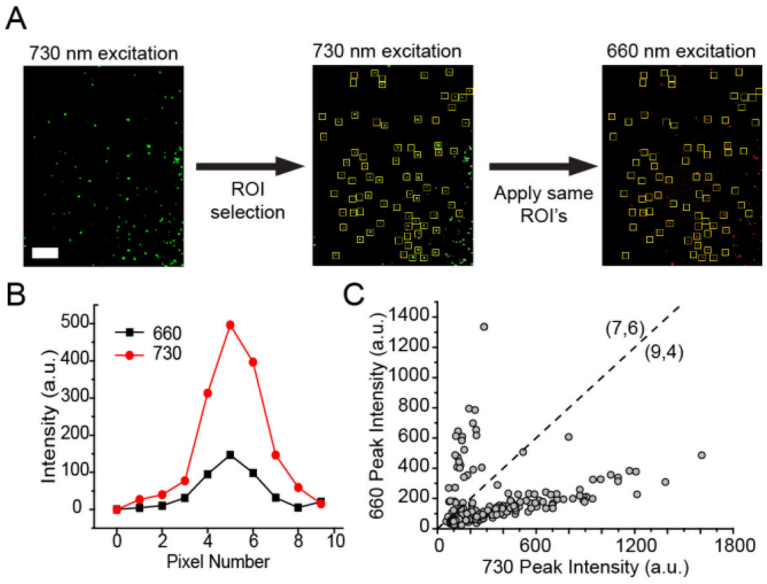


**Figure 4.**

Dual-excitation near-infrared fluorescence microscopy of single nanotubes to determine chiral purity. A) A representative field of view under 730 nm or 660 nm excitation, with selected ROIs shown. Scale bar = 10 μm. B) The intensity line profile of an individual nanotube under 730 nm and 660 nm excitation. C) Graph comparing the peak emission height of each selected ROI under 730 nm and 660 nm excitation.

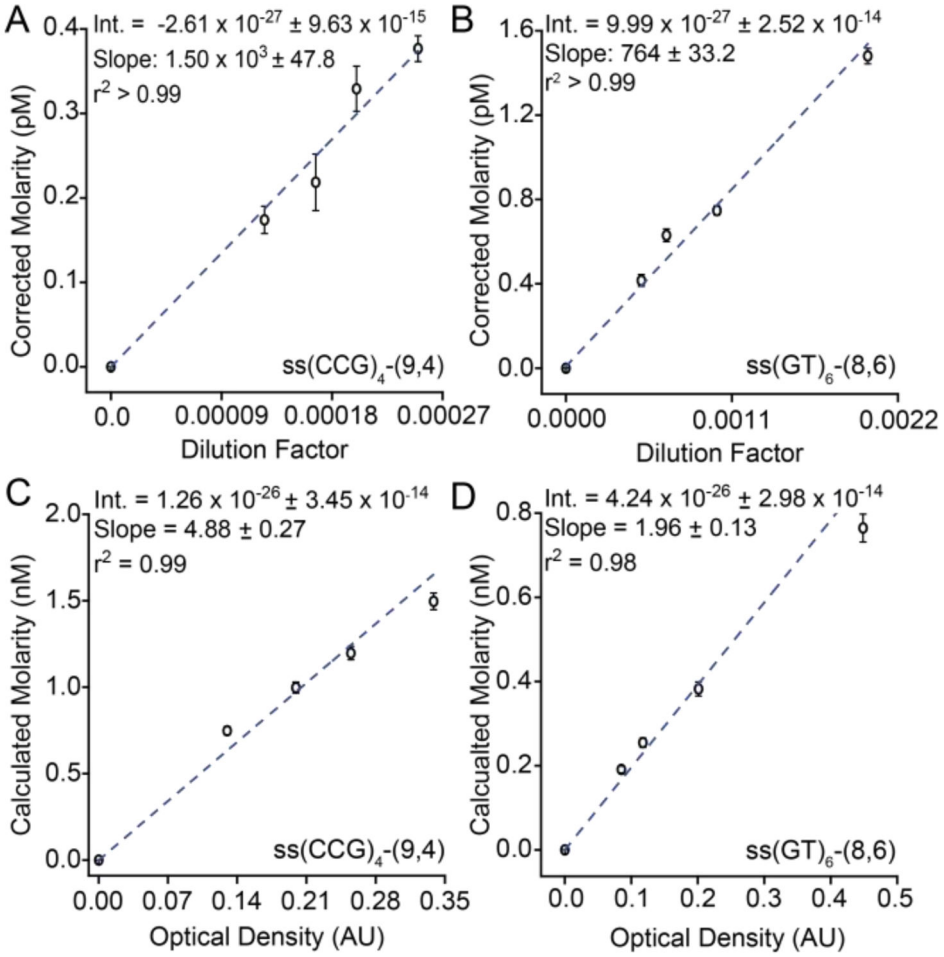


**Figure 5.**

Linear relation between nanotube concentration, deduced via microscopy, and the dilution factor or optical density of each sample. A) Corrected molarity vs. dilution factor for the (9,4) sample. B) Corrected molarity vs. dilution factor for the (8,6) sample. C) Calculated molarity vs. OD of the $E_{11}$ absorption peak for the (9,4) nanotube. D) Calculated molarity vs. OD of the $E_{11}$ absorption peak for the (8,6) nanotube.